A novel suspensible $TiB_{0.03}O_2$(y)/GB composite photocatalyst for azophloxine degradation

MEIHUA LIAN, YUXUAN LIU, WENJIE ZHANG*
School of Environmental and Chemical Engineering, Shenyang Ligong University, Shenyang 110159, China

A suspensible $TiB_{0.03}O_2$(y)/GB composite photocatalyst was synthesized by loading boron-doped TiO_2 on the glass bubbles via a sol-gel route. Characterization results proved the loading of anatase TiO_2 on the surface of the glass bubbles. The photocatalytic degradation of azophloxine on the materials was examined to show the effects of supporting. The density of the $TiB_{0.03}O_2$(y)/GB composites could be controlled by adjusting $TiB_{0.03}O_2$ loading content. Solid-water separation was easy since the material could float on the water surface after treatment. The $TiB_{0.03}O_2$(y)/GB composites were as active as $TiB_{0.03}O_2$ fine powders on azophloxine degradation. All the dye molecules were degraded after 180 min of reaction using either $TiB_{0.03}O_2$ or $TiB_{0.03}O_2$(50)/GB. The constituents in azophloxine solution during degradation were determined using UV-visible spectrometry. The major organic groups in azophloxine were decomposed during the degradation process.

(Received December 20, 2019; accepted April 7, 2021)

Keywords: TiO_2, Photocatalytic, Azophloxine, Degradation

1. Introduction

Industrial wastewater may contain various kinds of hazardous organic pollutants, and therefore, purification of industrial wastewater is necessary. Traditional biochemical treatment is widely used for organic pollutants. After half a century of investigations on basic theory and application technique, photocatalytic oxidation of organic pollutants has become a promising purification method for hazardous industrial wastewater [1-5]. Most kinds of organic pollutants can be removed from wastewater during photocatalytic oxidation process [6-8].

During development of photocatalytic oxidation technique, photocatalytic material is always the research focus. Titania based materials have been deeply studied in half a century [9-11]. Besides the investigation on fundamental properties of pure TiO_2, modification is applied to improve the activity of titania [12-15]. One of the most accepted modification methods is doping of metal or nonmetal ions in anatase TiO_2 [16-18]. For example, boron was reported to be a promising dopant in anatase TiO_2 skeleton to promote photocatalytic activity [19-21]. Boron doped TiO_2 was used as photocatalytic material instead of pure TiO_2 in this work.

Powder photocatalyst usually has high activity in wastewater treatment because fine material powder can be suspended well in wastewater. This is beneficial to both adsorption of organic pollutants and absorption of irradiation photons. However, fine powders are quite difficult to be removed from water. Since photocatalytic materials must be reused in large scale wastewater treatment plant, the materials need to be quickly removed from water after treatment. Photocatalytic materials are usually supported on plat substrates or solid materials with high density, but the supported materials are not as active as the fine powders. Hollow materials can be suspended in wastewater under gentle mixing or aeration if the density of the hollow materials is as similar as water. Some kinds of photocatalyst in the suspended form were reported recently [22-24]. Photocatalyst-water separation could be finished in a short time.

In this work, we reported the photocatalytic degradation of azophloxine on the suspensible $TiB_{0.03}O_2$(y)/GB composites. The composites were synthesized by loading boron-doped TiO_2 on the glass bubbles via a sol-gel route. The materials were characterized using scanning electron microscopy, transmission electron microscopy, and X-ray powder diffraction. The degradation of azophloxine in the solution was examined to study the activity of the materials.

2. Experimental methods

2.1. Preparation of $TiB_{0.03}O_2$(y)/GB

The average diameter of the glass bubbles (GB, 3M^{TM}) was 20 μm. The $TiB_{0.03}O_2$(y)/GB were synthesized by loading boron-doped TiO_2 on the glass bubbles via a sol-gel route. Tributyl borate (0.09 mL), tetrabutyl titanate (4 mL), hydrochloric acid (0.2 mL) and anhydrous ethanol (16 mL) were mixed to obtain solution A. Pure water (1.8 mL), glass bubbles, and anhydrous ethanol (8 mL) were mixed to prepare solution B. The two solutions were mixed to obtain a transparent sol, and the sol turned into a gel after 30 min. The gel was dehydrated at 80 ^oC, and the

gel was calcined at 450 °C for 3 h. The calcination product was ground into fine powder. In this work, the materials were named as $TiB_{0.03}O_2$(y)/GB. Here, y was referred to the weight percentage of $TiB_{0.03}O_2$ in the material. The atomic ratio of *n*(B)/*n*(Ti) was 0.03:1 in the materials.

2.2. Characterization methods

The XRD pattern of the material was taken on a D8 Advance X-ray diffractometer (Cu Kα, λ=1.5416Å). The SEM image of surface morphology was obtained by a QUANTA 250 scanning electron microscope. The TEM image of the material was taken on a FEI Tecnai G2 20 transmittance electron microscope.

2.3. Photocatalytic activity measurement

Azophloxine solution (50 mL, 40 mg/L) and 30 mg $TiB_{0.03}O_2$ were stirred in the dark for 30 min, and the concentration of azophloxine solution was measured to calculate the adsorption percent of azophloxine on the material. The photocatalytic degradation of azophloxine was evaluated after turning on a 20 W UV lamp (253.7 nm). The solid material was removed from the solution, and then the absorption intensity of the solution was recorded by a 721E spectrophotometer at the maximum absorption wavelength of 505 nm. The UV-vis spectra of the solution were recorded by a LAMBDA 35 UV-vis spectrometer. The produced hydroxyl radical after 30 min UV light exposure was measured in 0.5 mmol/L terephthalic acid solution. The solution was irradiated at 315 nm in a fluorescence spectrophotometer (LS-55).

3. Results and discussion

3.1. Characterization of $TiB_{0.03}O_2$(y)/GB

Fig. 1 shows the XRD patterns of $TiB_{0.03}O_2$ and $TiB_{0.03}O_2$(y)/GB composites. The glass bubbles were composed of soda-lime-borosilicate glass, which did not have characteristic diffraction peaks in the XRD pattern. The only phase in the $TiB_{0.03}O_2$(y)/GB composites was anatase TiO_2. All the diffraction peaks agreed with JCPDS 01-562. The diffraction intensity of the $TiB_{0.03}O_2$(50)/GB was lower than the diffraction intensity of $TiB_{0.03}O_2$, due to 50% content of $TiB_{0.03}O_2$ in the $TiB_{0.03}O_2$(50)/GB composite. The preferred orientation at diffraction angle of 2θ=25.2° indicates the (101) plane of tetragonal anatase TiO_2.

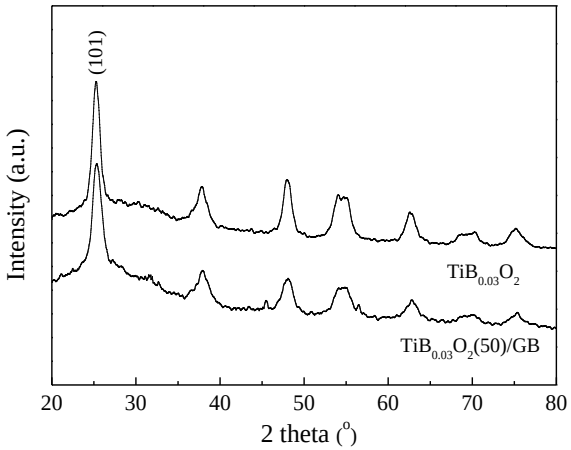

Fig. 1. XRD patterns of $TiB_{0.03}O_2$ and $TiB_{0.03}O_2$(50)/GB composite

Fig. 2 shows the SEM image and EDS titanium mapping of the $TiB_{0.03}O_2$(50)/GB composite. The glass bubbles were in the size between 10 and 20 μm. $TiB_{0.03}O_2$ was coated on the surface of the glass bubbles in a thin layer. However, the aggregation of $TiB_{0.03}O_2$ crystals into large particles is not avoidable in the $TiB_{0.03}O_2$(50)/GB sample due to high content of $TiB_{0.03}O_2$. As shown in Fig. 2(b), the EDS mapping of titanium in the sample proved the loading of $TiB_{0.03}O_2$ on the glass bubbles. Titanium element was observed on the entire surface of the $TiB_{0.03}O_2$(50)/GB composite.

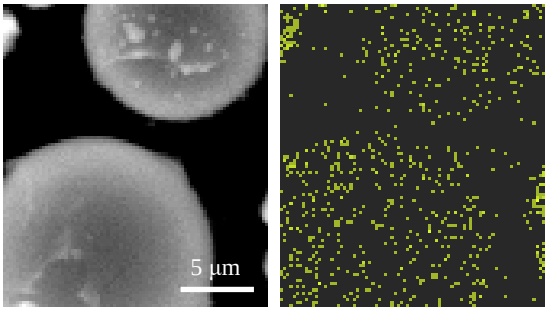

Fig. 2. EDS elemental mapping of titanium in $TiB_{0.03}O_2$(50)/GB composite (color online)

Fig. 3a shows the TEM image of small $TiB_{0.03}O_2$ particles. The nanosized $TiB_{0.03}O_2$ crystals intended to aggregate into large particles, and the interconnection of the crystals was clarified in the TEM image of the highly dispersed $TiB_{0.03}O_2$ particles. Fig. 3b gives the TEM cross-section image of $TiB_{0.03}O_2$(50)/GB composite to show the loading of $TiB_{0.03}O_2$ layer on the surface of the glass bubble. As shown in the figure, $TiB_{0.03}O_2$ was loaded on the surface of the glass bubble. The interaction between $TiB_{0.03}O_2$ layer and the glass bubble was tight, and the surface of the $TiB_{0.03}O_2$(50)/GB composite became rough due to the variation of the thickness of the $TiB_{0.03}O_2$ layer.

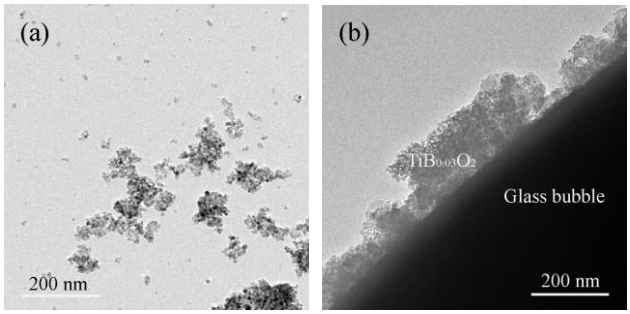

Fig. 3. (a) TEM image of small $TiB_{0.03}O_2$ particles, (b) TEM cross-section image of $TiB_{0.03}O_2$(50)/GB composite to show the loading of $TiB_{0.03}O_2$ layer on the glass bubble

3.2. Hydroxyl radical production

The initial step of a photocatalytic process is the excitation of a valence band electron to the conduction band, leaving a hole in the conduction band. The holes and electrons have enough power to produce the oxidative species, e.g. hydroxyl radical [25-27]. Terephthalic acid can react with hydroxyl radical to produce 2-hydroxy-terephthalic acid. Fig. 4 shows the fluorescence spectra of 2-hydroxy-terephthalic acid solution after 30 min of irradiation in presence of the $TiB_{0.03}O_2$(y)/GB composites. The sequence of fluorescence intensity indicates the photocatalytic activity of the $TiB_{0.03}O_2$(y)/GB composites.

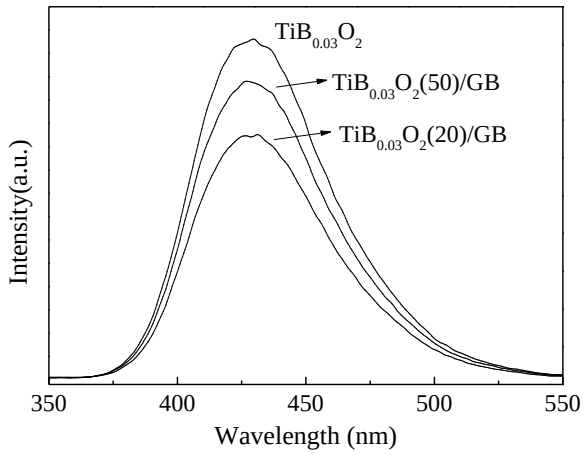

Fig. 4. Fluorescence spectra of 2-hydroxy-terephthalic acid solution after 30 min of photocatalytic generation of hydroxyl radicals on the $TiB_{0.03}O_2$(y)/GB composites

3.3. Photocatalytic degradation of azophloxine

The density of the glass bubbles was 0.46 g/cm^3, and the crush strength of the glass bubbles at 90% survival by volume was 16000 psi. These glass bubbles were used in industrial applications to reduce part weight and enhance product properties. The function of the low-density glass bubbles in this work was to lower the density of boron-doped TiO_2 photocatalyst. We prepared a series of supported $TiB_{0.03}O_2$(y)/GB samples with different $TiB_{0.03}O_2$ loading content. The density of $TiB_{0.03}O_2$(20)/GB was 0.73 g/cm^3, and the density of $TiB_{0.03}O_2$(50)/GB was 0.96 g/cm^3. The density of the supported $TiB_{0.03}O_2$(y)/GB was slighter than water, so that the material could be suspended well in water under mixing or aeration to accomplish purification process. Solid-water separation was easy since the $TiB_{0.03}O_2$(y)/GB composites floated on the water surface after treatment.

Fig. 5 shows the decoloration of azophloxine on the $TiB_{0.03}O_2$(y)/GB composites to study the effects of $TiB_{0.03}O_2$ loading content. The glass bubbles did not have activity on azophloxine decoloration, neither through photocatalytic degradation nor by adsorption. The adsorption of azophloxine on the $TiB_{0.03}O_2$(y)/GB composites was less than 1.4%. After 30 min of photocatalytic oxidation, azophloxine degradation efficiency increased with rising $TiB_{0.03}O_2$ loading content. When $TiB_{0.03}O_2$ loading content was more than 50%, the photocatalytic activity of $TiB_{0.03}O_2$(50)/GB was almost as same as the unsupported $TiB_{0.03}O_2$ powders. As reported in many literatures, supporting of photocatalytic material usually leads to a reduced activity. The finding in this work was interesting that the $TiB_{0.03}O_2$(y)/GB composites were as active as $TiB_{0.03}O_2$ fine powders. The $TiB_{0.03}O_2$(y)/GB composites were regarded as a promising potential photocatalyst in large scale wastewater treatment.

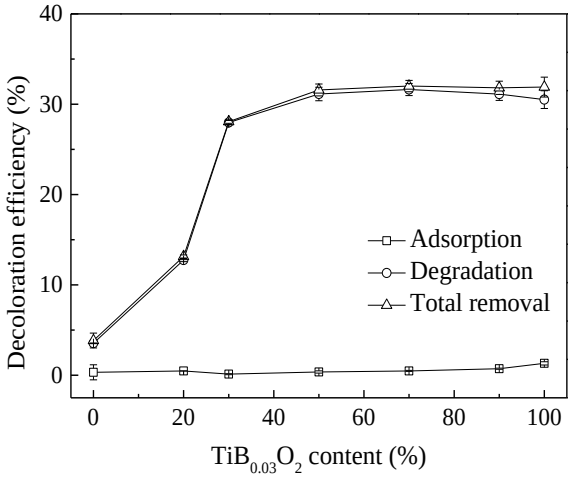

Fig. 5. Decoloration efficiency of azophloxine on $TiB_{0.03}O_2$(y)/GB composites with respect to $TiB_{0.03}O_2$ loading content. The irradiation time was 30 min for photocatalytic degradation of azophloxine

Fig. 6a shows the photocatalytic degradation of azophloxine on the $TiB_{0.03}O_2$(y)/GB composites with extended irradiation time. Decoloration of azophloxine was mostly attributed to degradation of the dye since the adsorption percentage of azophloxine on the material was quite small. The azophloxine molecules were constantly decomposed during the photocatalytic process. All the dye molecules were degraded after 180 min of reaction using either $TiB_{0.03}O_2$ or $TiB_{0.03}O_2$(50)/GB. Fig. 6b illustrates the kinetic plots of photocatalytic degradation of azophloxine on the $TiB_{0.03}O_2$(y)/GB composites. Photocatalytic

degradation of azophloxine followed the kinetic law of a first order reaction. The first order reaction rate constants were 0.0051, 0.0277 and 0.0308 min^{-1} for the photocatalytic degradation of azophloxine on the $TiB_{0.03}O_2$(20)/GB, $TiB_{0.03}O_2$(50)/GB and $TiB_{0.03}O_2$, respectively.

Photocatalyst in fine particles had a high activity while the material might lose a part of activity after supporting. Since photocatalytic reaction occurred on the external surface of photocatalyst, the valid surface of photocatalyst was essential to both adsorption of organic substance and absorption of incoming photons. The glass bubbles were not transparent to ultraviolet light, and they might inhibit the transmission of UV photons into deep water. This was the reason that $TiB_{0.03}O_2$(20)/GB had a weaker activity than the other two samples. The density of the $TiB_{0.03}O_2$(y)/GB composites could be adjusted by changing $TiB_{0.03}O_2$ loading content. If $TiB_{0.03}O_2$ loading content was low, the light $TiB_{0.03}O_2$(y)/GB particles tended to float on top water surface to screen the incoming photons. When $TiB_{0.03}O_2$ loading content was higher than 30%, the activity of $TiB_{0.03}O_2$(y)/GB was as similar as the unsupported $TiB_{0.03}O_2$ powders.

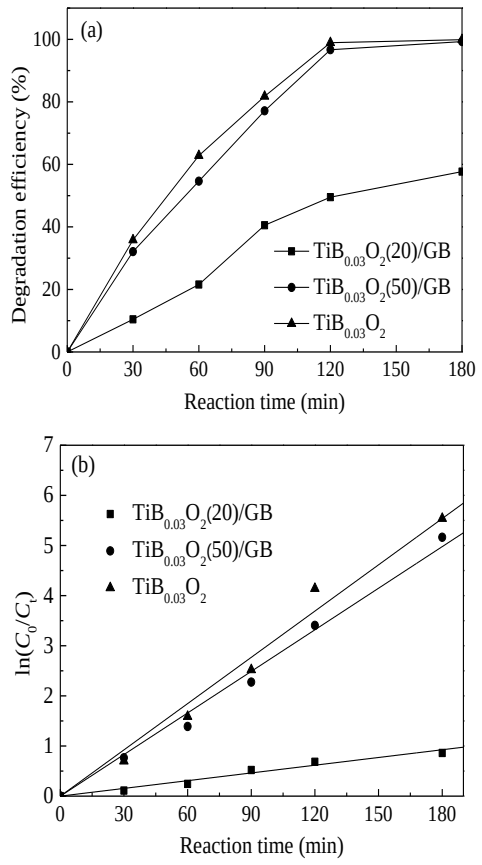

Fig. 6. (a) Photocatalytic degradation of azophloxine on $TiB_{0.03}O_2$(y)/GB composites with extended irradiation time, and (b) Kinetic plots of photocatalytic degradation of azophloxine on $TiB_{0.03}O_2$(y)/GB

The unsupported $TiB_{0.03}O_2$ powders were composed of aggregated $TiB_{0.03}O_2$ particles whose activity depended on the particle size. Small particles might have high activity due to the large surface area. However, the smaller in particle size, the greater in difficulty for photocatalyst-water separation after treatment. Loading of $TiB_{0.03}O_2$ on the glass bubbles deposited a thin layer of $TiB_{0.03}O_2$ on the external surface of the hollow glass bubbles. The positive influences of supporting photocatalyst were discussed in the literatures [22-24], mostly due to enlarged specific surface area of the supported photocatalytic materials. Interestingly, the novelty of this work was that not only the supported $TiB_{0.03}O_2$(y)/GB composites had a high activity, but also the materials were easily removed from water.

Fig. 7 (a-c) illustrate the UV-vis spectra of azophloxine solution during degradation on the $TiB_{0.03}O_2$(y)/GB with different loading content. Fig. 6d shows the UV-vis spectra of azophloxine solution after 30 min of degradation on different samples. The strong absorption band in the visible region was the character of the azo dye, indicating the chromophore group. The original azophloxine solution had the maximum absorption intensity at 505 nm. There were four absorption peaks in the ultraviolet region for the azophloxine solution. The strong absorption peak at 235 nm was attributed to the intrinsic absorption of the benzene ring and naphthalene ring, while the weak absorption peak at 249 nm was due to the n-π conjugated absorption of the secondary amide. The absorptions at 364 nm and 312 nm were related to the interplay of the benzene ring and naphthalene ring with the chromophore group.

The absorption intensity of the peaks in both visible and ultraviolet region shrank with extended irradiation time, indicating decomposition of the functional groups in the azophloxine molecule. The decrease in absorption intensity was more obvious for the solution containing $TiB_{0.03}O_2$(50)/GB or $TiB_{0.03}O_2$. After 180 min of reaction, almost all the absorption peaks disappeared in the spectra, showing overall decomposition of the major groups in the azo dye. Besides the organic substituent involved in the degradation intermediates of azophloxine, the dye had an apparent environmental defect of the color. The color of dye came from absorption in the visible region by the azo chromophore group. We cannot assure that the dye was completely degraded until all the functional groups in the dye were broken up. As shown in Fig. 7b and 7c, there was no absorption in the spectra more than 220 nm. The major organic groups in azophloxine, such as the chromophore group, the secondary amide, the benzene ring and naphthalene ring were decomposed.

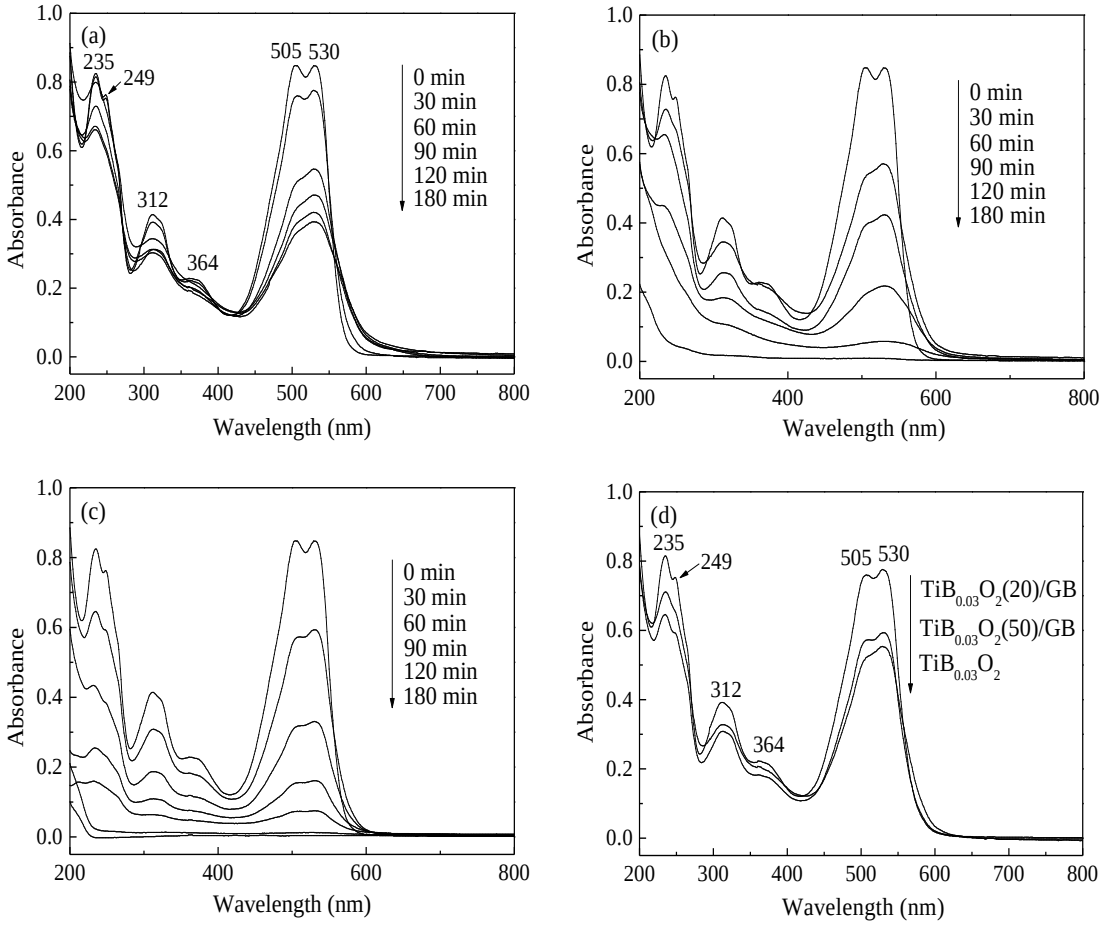

Fig. 7. UV-vis spectra of azophloxine solution during degradation on $TiB_{0.03}O_2$(y)/GB with different loading content. (a) $TiB_{0.03}O_2$(20)/GB, (b) $TiB_{0.03}O_2$(50)/GB, (c) $TiB_{0.03}O_2$, (d) UV-vis spectra of azophloxine solution after 30 min of degradation on different samples

4. Conclusions

The $TiB_{0.03}O_2$(y)/GB composites were synthesized by loading boron-doped TiO_2 on the glass bubbles via a sol-gel route. The photocatalytic degradation of azophloxine in the solution was examined on the $TiB_{0.03}O_2$(y)/GB composites. The density of the supported $TiB_{0.03}O_2$(y)/GB was lower than water, and therefore, the material was suspended well in water. When $TiB_{0.03}O_2$ loading content was higher than 30%, the activity of $TiB_{0.03}O_2$(y)/GB composites was as strong as the unsupported $TiB_{0.03}O_2$ powders. The UV-vis spectra proved the degradation of azophloxine during the photocatalytic oxidation process.

Acknowledgments

This work was supported by the Scientific Research Fund of Liaoning Provincial Education Department (No. LG201923).

References

[1] M. R. Hoffmann, S. T. Martin, W. Choi, W. Bahnemann, Chem. Rev. **95**, 69 (1995).
[2] S. Zinatloo-Ajabshir, Z. Salehi, M. Salavati-Niasari, J. Clean. Prod. **192**, 678 (2018).
[3] A. Fujishima, T. N. Rao, D. A. Tryk, J. Photochem. Photobio. C **1**, 1 (2000).
[4] Y. J. Wang, Q. Y. Wang, H. Zhang, Y. Wu, Y. Jia, R. C. Jin, S. M. Gao, Sep. Purif. Technol. **242**, 116775 (2020).
[5] A. Kaur, G. Gupta, A. O. Ibhadon, D. B. Salunke, A. S. K. Sinha, S. K. Kansal, J. Environ. Chem. Eng. **6**, 3621 (2018).
[6] Z. Y. Liu, Y. D. Song, Q. Y. Wang, Y. Jia, X. Y. Tan, X. X. Du, S. M. Gao, J. Colloid Interf. Sci. **556**, 92 (2019).
[7] E. Hapeshi, A. Achilleos, M. I. Vasquez, C. Michael, N. P. Xekoukoulotakis, D. Mantzavinos, D. Kassinos, Water Res. **44**, 1737 (2010).
[8] W. J. Zhang, Y. J. Tao, C. G. Li, J. Photochem.

Photobio. A: Chem. **364**, 787 (2018).
[9] C. T. Chekem, V. Goetz, Y. Richardson, G. Plantard, J. Blin, Catal. Today **328**, 183 (2019).
[10] Z. D. Mahmoudabadi, E. Eslami, J. Alloys. Compd. **793**, 336 (2019).
[11] R. M. Mohamed, A. A. Ismail, M. W. Kadi, D. W. Bahnemann, J. Photochem. Photobio. A: Chem. **367**, 66 (2018).
[12] C. Bogatu, M. Covei, D. Perniu, I. Tismanar, A. Duta, Catal. Today **328**, 79 (2019).
[13] Y. Jia, P. B. Liu, Q. Y. Wang, Y. Wu, D. D. Cao, Q. A. Qiao, J. Colloid Interf. Sci. **585**, 459 (2021).
[14] D. D. Cao, Q. Y. Wang, Y. Wu, S. X. Zhu, Y. Jia, R. L. Wang, Sep. Purif. Technol. **250**, 117132 (2020).
[15] O. Sacco, V. Vaiano, C. Daniel, W. Navarra, V. Venditto, Mater. Sci. Semicond. Proce. **80**, 104 (2018).
[16] A. Zielińska-Jurek, I. Wysocka, M. Janczarek, W. Stampor, J. Hupka, Sep. Purif. Technol. **156**, 369 (2015).
[17] M. Nasirian, M. Mehrvar, J. Environ. Sci. **66**, 81 (2018).
[18] Q. Y. Wang, H. L. Li, X. L. Yu, Y. Jia, Y. Chang, S. M. Gao, Electrochim. Acta **330**, 135167 (2020).
[19] W. Zhang, X. Pei, B. Yang, H. He, J. Adv. Oxid. Technol. **17**, 66 (2014).
[20] E. B. Simsek, Appl. Catal. B: Environ. **200**, 309 (2017).
[21] W. Zhang, Y. Liu, H. Xin, Curr. Nanosci. **14**, 209 (2018).
[22] B. Cao, G. Li, H. X. Li, Appl. Catal. B: Environ. **194**, 42 (2016).
[23] G. H. Sun, C. S. Zhu, J. T. Zheng, B. Jiang, H. C. Yin, H. Wang, S. Qiu, J. J. Yuan, M. B. Wu, W. T. Wu, Q. Z. Xue, Mater. Lett. **166**, 113 (2016).
[24] W. J. Zhang, Y. J. Tao, C. G. Li, Mater. Res. Bull. **105**, 55 (2018).
[25] Z. Y. Liu, Q. Y. Wang, D. D. Cao, Y. J. Wang, R. C. Jin, S. M. Gao, J. Alloy. Compds. **820**, 153109 (2020).
[26] Z. Y. Liu, Q. Y. Wang, X. Y. Tan, S. X. Zheng, H. Zhang, Y. J. Wang, S. M. Gao, J. Alloy. Compds. **815**, 152478 (2020).
[27] Z. Y. Liu, Q. Y. Wang, X. Y. Tan, Y. J. Wang, R. C. Jin, S. M. Gao, Sep. Purif. Technol. **215**, 565 (2019).

*Corresponding author: wjzhang@aliyun.com